Journal of Thermal Analysis and Calorimetry, Vol. 80 (2005) 477–482

# REFUSE DERIVED FUELS PYROLYSIS
## Influence of process temperature on yield and products composition

*S. Casu, S. Galvagno, A. Calabrese, G. Casciaro, M. Martino, A. Russo and Sabrina Portofino* *

ENEA Trisaia Research Centre, 75026 Rotondella (MT), Italy

Refuse derived fuels (RDF) characterization and pyrolysis behaviour, carried out by means of thermogravimetric analysis, infrared and mass spectroscopy, are presented. Thermal degradation of RDF takes place through three main mass loss stages; the analyses of evolved gas allow us to discriminate the contributions of the different fractions (paper, LDPE, wood, rubber, etc.) to the global decomposition. Furthermore thermogravimetry (TG) was used for the determination of kinetic parameters, using the differential method.

In order to set up the conditions of production of a good quality pyrolysis gas, the operating conditions of RDF in a pyrolysis reactor have been simulated. Data show that the volatile fraction grows with the temperature, together with the relative conversion, and that light volatile fraction (hydrogen, ethyne, etc.) gets richer, at the expense of superior homologous hydrocarbons.

***Keywords:*** *process temperature, pyrolysis, refuse derived fuels, TG/FTIR/MS*

## Introduction

Italian decree law 22/97 has acknowledged European strategies on waste management (minimization, reuse, recycling and recovery). In this context such decree, in order to promote a ruled energetic exploitation of waste, introduced CDR, a kind of refuse derived fuel (RDF) whose characteristics are properly defined throughout the same decree.

Nevertheless, up to now, RDF utilization has disappointed the expectations, on one end because of the strict law limits that regulate the production, on the other because of the heterogeneity of its composition that bounds its exploitation.

Since the opportunity to use RDF to produce fuel gas seems to be promising, particular attention has been focused on process technologies such as pyrolysis and gasification [1].

Present work relates to experimental tests and obtained results of the study of RDF performance, carried out by means of thermogravimetry (TG), infrared and mass spectrometry, in order to characterize the incoming material and to establish the best condition of fuel gas production.

## Experimental

### *Materials*

Samples used for the experimental work are commercial products, supplied by an Italian producer. Because of the high moisture content of RDF, about 25–30%, it was necessary to dry the samples before they were milled till to a size of maximum 0.2 mm.

After grinding, samples were kept at ambient conditions.

### *Apparatus and procedures*

A TA TG 2950 system, coupled with a Thermo Optek FTIR spectrometer and a Thermo Onix quadrupole mass spectrometer, were used to perform thermal analyses and for on-line monitoring of evolved gas fraction.

Thermogravimetric curves have been recorded at four different heating rates (5, 10, 20 and 50 K $min^{-1}$) and at three process temperatures (600, 700 and 800°C). Pure nitrogen was used as inert purge gas, at constant flow rate of 100 mL $min^{-1}$ [2, 3].

Ultimate analyses were obtained with a ThermoQuest EA 1110 analyser.

## Results and discussion

Proximate and ultimate analyses of the RDF are shown in Table 1; the data indicate a very high volatile content (up to 80%) and an ash quantity of 14%. As we see from the ultimate analysis, the material presents a good carbon quantity, while there's no evidence of the presence of either sulphur or chlorine.

Mass loss curves during RDF pyrolysis were obtained both in isothermal and constant heating rate conditions. The evolution profile of RDF samples from TG-DTG in nitrogen atmosphere from 100

* Author for correspondence: sabrina.portofino@trisaia.enea.it

1388–6150/$20.00

Akadémiai Kiadó, Budapest, Hungary
Springer, Dordrecht, The Netherlands

**Table 1** Characteristics of RDF*

| Element | Composition/% | Proximate analysis/% | | GHV/MJ kg$^{-1}$ |
|---|---|---|---|---|
| C | 51.0 | volatile matter | 78.6 | 27.6 |
| H | 7.3 | fixed carbon | 7.4 | |
| N | 0.8 | ash | 14.0 | |

*on dry basis

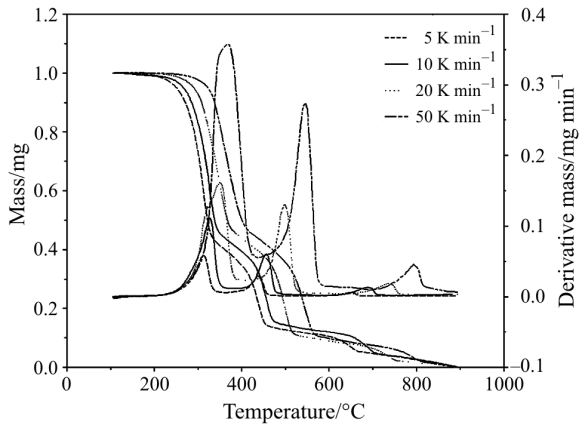


**Fig. 1** TG and DTG curves of RDFat different heating rates

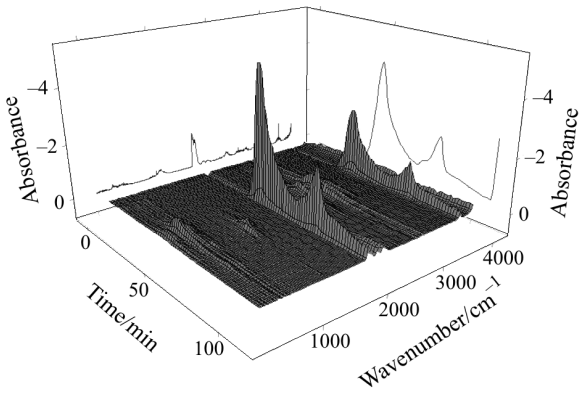


**Fig. 2** FTIR series of evolved gas

to 900°C, at different heating rate, is reported in Fig. 1 (data have been normalised with respect to moisture and ash content).

The curves show that the thermal decomposition is almost completed around 800°C; such decomposition takes place through a series of complex peaks related to the simultaneous degradation of the various fractions (paper, plastics, wood, fabrics, etc.) contained in RDF. Three main mass loss stages are found: the DTG curves show that the maximum pyrolysis reaction rate occurred at 312–360°C in the first reaction, at 430–540°C in the second reaction and above 650°C in the last reaction. The comparison with TG curves for the pyrolysis of paper, LDPE, wood, etc., and the analysis of evolved gas from FTIR/MS let us ascribe the first and the third peak to the decomposition of cellulose and ligneous materials; the peak in the medium region is more likely due to the decomposition of plastics, mainly LDPE [4–7].

The examination of FTIR series (Fig. 2) points out the presence, among the evolved gases, of water, carbon monoxide, carbon dioxide, methanol, acetic aldehyde, acetic acid, methane, ethylene, propylene, ethyne, aliphatic hydrocarbons, benzene. Such species have been detected as well by monitoring mass spectra of gaseous stream, together with hydrogen, not FTIR sensible (Table 2).

Without any separation of the fractions (such as a chromatographic separation), a definitive identification of components is quite difficult; nevertheless the comparative analysis of FTIR/MS spectra *vs*. time/temperature can confirm the attribution of the decomposition reactions from thermogravimetric curves mentioned above. As a matter of fact, *m*/*e* 44 trend (Fig. 3a) shows a peak around 320°C, comparable with $CO_2$ FTIR profile (Fig. 3b); in the same way, *m*/*e* 29 (–CHO), *m*/*e* 31 (–$CH_3O$) and *m*/*e* 43 ($CH_3OC$–) peaks fit the corresponding profiles coming out for methanol, acetic acid and acetaldehyde from FTIR series, and all the peaks fall in the same temperature range (Figs 3c and d). All these data confirm the hypothesis of attribution of the first decomposition peak to the degradation of cellulose and the other lignocellulosic materials.

**Table 2** FTIR and MS signals of evolved gas

| | Main FTIR signal (cm$^{-1}$) | Main MS signal (*m*/*e*) |
|---|---|---|
| $H_2O$ | 3790 | 18 |
| $H_2O$ | – | 2 |
| CO | 2480 | 28 |
| $CO_2$ | 2358 | 44 |
| $CH_3OH$ | 1032 | 31 |
| $CH_3CHO$ | 1760 | 29, 43 |
| $CH_3COOH$ | 1796 | 31, 43 |
| $CH_4$ | 3017 | 15, 16 |
| $C_2H_4$ | 949 | 28 |
| $C_3H_6$ | 911 | 41, 42 |
| $C_2H_2$ | 731 | 26 |
| –CH | 2936–2969 | 41, 42, 55, 56 |
| $C_6H_6$ | 670 | 78 |

With respect to the second pyrolysis reaction, we register, in the range of 400–450°C, the same agreement between the *m*/*e* trend and the FTIR spectra of ethylene, propylene, methane (Figs 3e–h), and other aliphatic compounds, coming from the decomposition of the plastic fraction [8–13].

Particular attention should be devoted to the analysis of mass spectrum of *m*/*e* 16; in comparison with the corresponding methane FTIR trend, we notice that both the traces show a peak centred around 450°C, while other two remarkable peaks, present in mass spectrum, are less representative throughout the FTIR profile. Such behaviour could be ascribed to the fragmentation spectrum of other species falling at the same *m*/*e* ratio: i.e., $CO_2$ *m*/*e* 16 peak is 6% of the main peak, at *m*/*e* 44, while $O_2$ *m*/*e* 16 peak is 4.2% with respect to the main peak. This interpretation is coherent with the $CO_2$ trends, as reported in Figs 3a and b, and with the

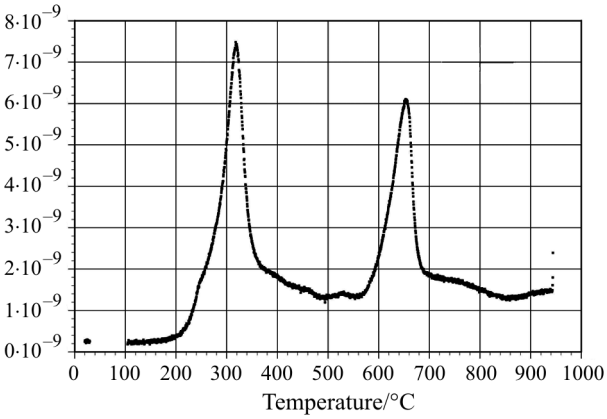


**Fig. 3a** *m*/*e* 44 trend

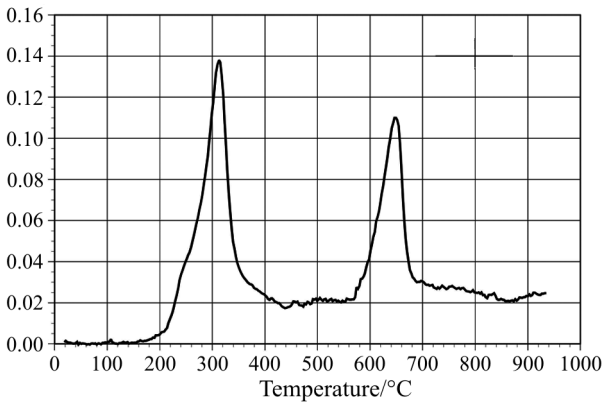


**Fig. 3b** $CO_2$ FTIR profile

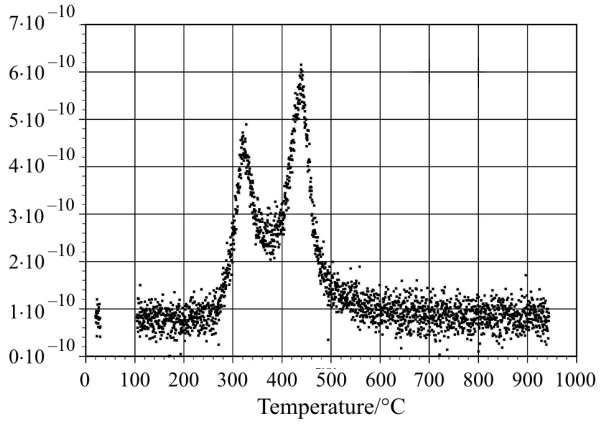


**Fig. 3c** *m*/*e* 43 trend

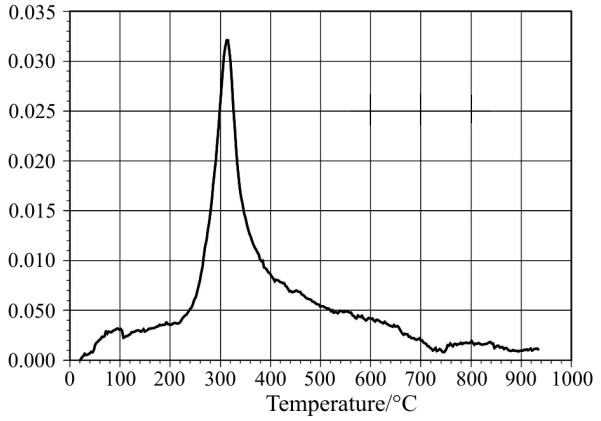


**Fig. 3d** Ethanal FTIR profile

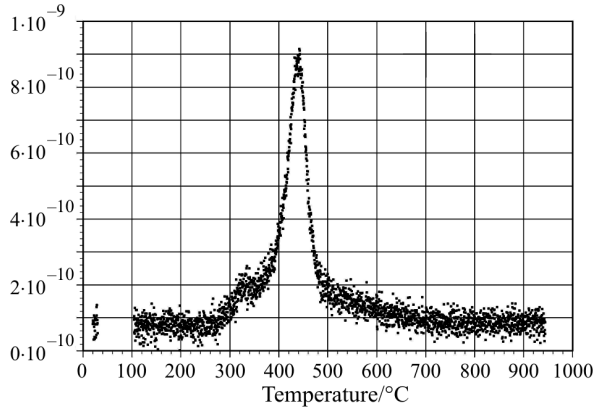


**Fig. 3e** *m*/*e* 41 trend

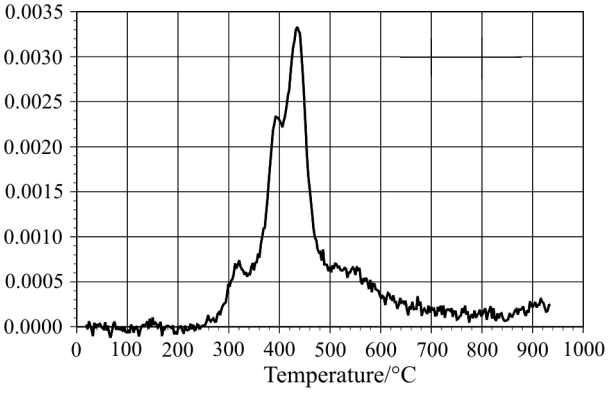


**Fig. 3f** Propylene FTIR profile

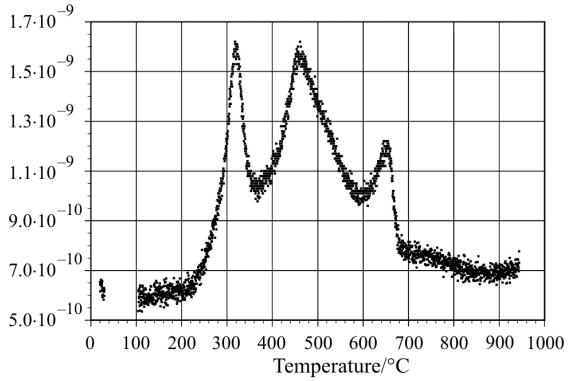


**Fig. 3g** *m*/*e* 16 trend

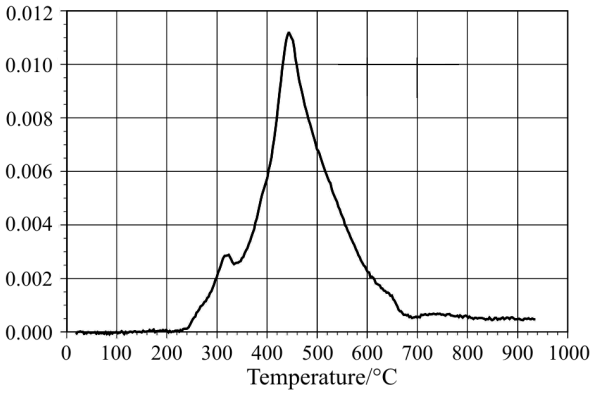


**Fig. 3h** Methane FTIR profile

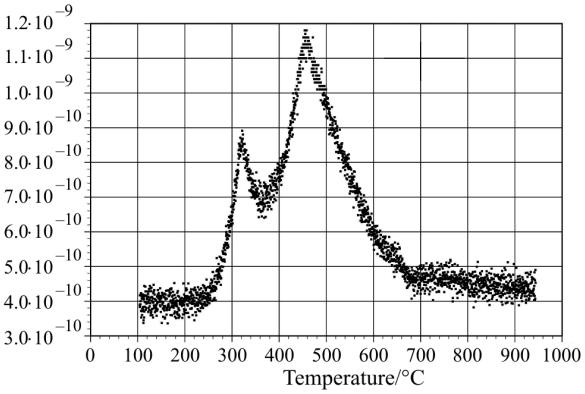


**Fig. 3i** *m*/*e* 15 trend

*m*/*e* 15 profile (Fig. 3i): as a matter of fact, *m*/*e* 15 peak is rather representative of the methane fragmentation path (its intensity being equal to 80% of main methane peak, at *m*/*e* 16); such peak is less influenced from the fragmentation of other species and is better comparable to the corresponding methane FTIR profile.

In order to have a better understanding of RDF pyrolysis, the determination of kinetic parameters was carried on employing the differential method [14–19].

The residual mass fraction of active reactant is expressed on a normalized basis, according to Eq. (1)

$$M=(W-W_f)/(W_0-W_f) \quad (1)$$

where $W$, $W_0$, $W_f$ represent mass, initial mass and final mass of the sample, respectively. The conversion $X$ is expressed as

$$X=(W_0-W)/(W_0-W_f) \quad (2)$$

where

$$M=1-X \quad (3)$$

Two principal reactions take place in the range $1<M<0.42$ and $0.42<M<0.10$, respectively. Both the reactions were studied assuming that

$$dX/dt=k(1-X)^n \quad (4)$$

and

$$k=A\exp(-E_a/RT) \quad (5)$$

Therefore the plots of $\ln(dX/dt)$ *vs*. $-1/T$, following Eqs (4) and (5), for different heating rates in iso-conversion conditions, give the activation energy (equals to 95.5 and 108.1 kJ mol$^{-1}$, for first and second reaction respectively, Table 3).

The reaction order ($n$) and the pre-exponential factor ($A$) were obtained plotting $\ln[(dX/dt)/\exp(-E_a/RT)]$ *vs*. $\ln(1-X)$.

In order to investigate the conditions of production of a good quality gas in a pyrolysis reactor, a series of TG/FTIR/MS tests have been performed, simulating the operating conditions of RDF in a continuous process, where the material comes in at a fixed temperature, and undergoes a fast heating, for a definite residence time. Process temperatures of 600, 700 and 800°C, chosen from the analysis of thermogravimetric curves, have been investigated.

Data in Table 4 show that the volatile fraction grows with the process temperature, together with the relative conversion. On-line FTIR and MS spectra of evolved gas monitored during the process, point out that, at growing temperature, light volatile fraction gets richer at the expense of aliphatic hydrocarbons;

**Table 3** Kinetic parameters

| Data | First reaction | Second reaction |
|---|---|---|
| $E_a$/kJ mol$^{-1}$ | 95.5 | 108.1 |
| $A$/min$^{-1}$ | $4.5\cdot10^7$ | $8.4\cdot10^6$ |
| $n$ | 2.2 | 0.7 |

**Table 4** Conversion data

| Data/% | RDF 600* | RDF 700* | RDF 800* |
|---|---|---|---|
| volatile matter at Tiso | 76.14 | 77.72 | 85.98 |
| total volatile matter | 91.04 | 80.68 | 88.22 |
| conversion | 83.63 | 96.33 | 97.46 |

*Dry ash free samples

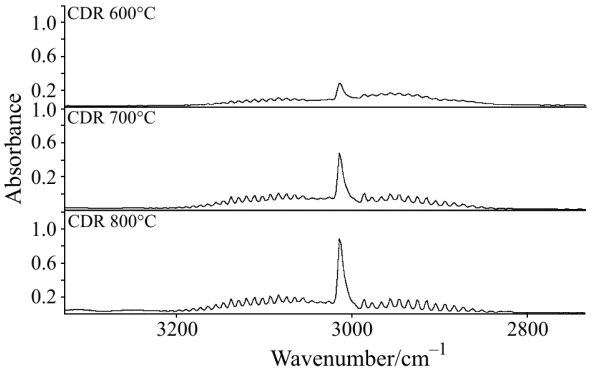


**Fig. 4a** FTIR curves of methane production at different process temperatures

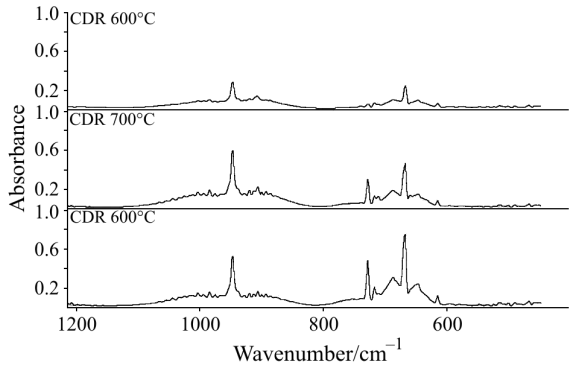


**Fig. 4b** FTIR curves of ethyne production at different process temperatures

as a matter of fact, FTIR signal at 2800–3200 cm$^{-1}$, related to aliphatic and aromatic absorption, goes down, while the peak of ethyne, at low wavenumber, definitely increases (Figs 4a, b). Furthermore, this fact means that at growing temperature condensable fraction (that is oils) lowers, moving the balance towards the incondensable fraction and providing a fuel gas of better quality.

Figure 5 shows the behaviour of various components in the volatile fraction at different temperature; as far as methane, CO, $CO_2$, ethylene and ethyne are concerned, the evaluation comes from the corresponding chemigrams area (that is the IR absorption intensity of a given signal *vs*. time), normalised with respect to total volatile content; as far as hydrogen and ethane are concerned, peaks of corresponding relative abundance coming from MS were used.

Such diagrams show that $CO_2$ production gets a maximum at 700°C and then goes down; while, CO production follows the opposite trend, according to the Boudouard equilibrium. Furthermore, as far as the series of C2 homologues is concerned, the progressive dehydrogenation with temperature is observed: ethane concentration decreases in favour of ethene, whose quantity, at rising temperature, will lower in favour of

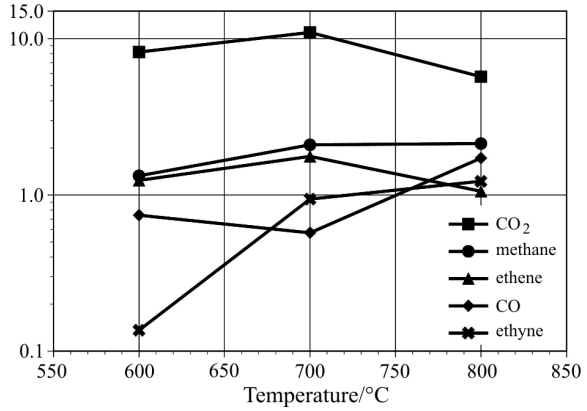


**Fig. 5a** Gas production *vs*. temperature, FTIR data

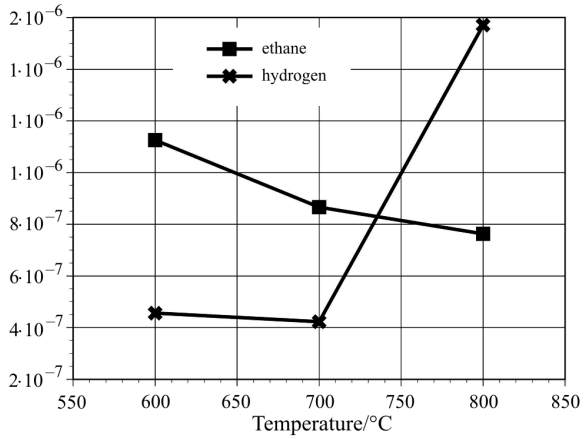


**Fig. 5b** Gas production *vs*. temperature, MS data

ethyne; for the same reasons, the hydrogen content registers a marked growth, showing a maximum at 800°C.

It is important to point out that the data are far to be quantitative, though they provide a comparative evaluation of how single gas component abundance vary with the process temperature.

## Conclusions

RDF pyrolysis tests have been carried out with the system TG/FTIR/MS; in order to characterize the thermal behaviour of such material; thermogravimetric curves showed that the decomposition reactions are definitely complete around 600°C (with a conversion over 80%). The experimental results show that two principal reactive steps take place, and the online monitoring of evolved gas let us ascribe the first step to the decomposition of cellulose and lignocellulosic material, the second one to the decomposition of plastic fraction.

In order to have a better understanding of RDF pyrolysis process, the determination of kinetic parameters for both steps was carried out using the differen-

tial method. Obtained data are in good agreement with similar values reported in other works.

The operating conditions of RDF in a pyrolysis reactor were simulated, at different process temperature, with the aim of setting up the conditions of production of a good quality pyrolysis gas. Data show that the volatile fraction grows with the temperature, together with the relative conversion, and that light volatile fraction (hydrogen, ethyne, etc.) gets richer, at the expense of superior homologous hydrocarbons.

## Abbreviations

| | |
|---|---|
| RDF, CDR | refuse derived fuels |
| $M$ | residual mass fraction |
| $X$ | conversion |
| $k$ | kinetic constant |
| $A$ | pre-exponential factor |
| $E_a$ | activation energy |
| $n$ | reaction order |

## Acknowledgments

This work was funded by ENEA and Italian Minister of Education, University and Scientific Research (Azione Organica 2 – L. 64/1986).

## References

1 N. Kiran, E. Ekinci and C. E. Snape, Res. Conserv. Recyc., 29 (2000) 273.
2 P. J. Haines, in Thermal Methods of Analysis, Ed. Chapman & Hall (1995), pp. 34–42.
3 J. Heikkinen and H. Spliethoff, J. Therm. Anal. Cal., 72 (2003) 1031.
4 A. N. Garcia, A. Marcilla and R. Font, Thermochim. Acta, 254 (1995) 277.
5 V. Cozzani, L. Petarca and L. Tognotti, Fuel, 75 (1995) 903.
6 M. Stenseng, A. Jensen and K. Dam-Johansen, J. Anal. Appl. Pyrolysis, 58–59 (2001) 765.
7 M. Müller-Hagedorn, H. Bockhorn, L. Krebs and U. Müller, J. Anal. Appl. Pyrolysis, 68–69 (2003) 231.
8 W. M. Groenewoud and W. de Jong, Thermochim. Acta, 286 (1996) 341.
9 D. M. Price and S. P. Church, Thermochim. Acta, 294 (1997) 107.
10 R. Lu, S. Purushothama, X. Yang, J. Hyatt, W.-P. Pan, J. T. Riley and W. G. Lloyd, Fuel Proc. Tech., 59 (1999) 35.
11 L. F. Calvo, M. E. Sánchez, A. Morán and A. I. Garcia, J. Therm. Anal. Cal., 78 (2004) 587.
12 T. Kaljuvee, J. Pelt and M. Radin, J. Therm. Anal. Cal., 78 (2004) 399.
13 T. Fisher, M. Hajaligol, B. Waymack and D. Kellogg, J. Anal. Appl. Pyrolysis, 62 (2002) 331.
14 M. S. Crespi, A. R. Silva, C. A. Ribeiro, S. C. Oliveira and M. R. Santiago-Silva, J. Therm. Anal. Cal., 72 (2003) 1049.
15 V. Mamleev, S. Bourbigot, M. Le Bras and J. Lefebvre, J. Therm. Anal. Cal., 78 (2004) 1009.
16 J. H. Chan and S. T. Balke, Polym. Degrad. Stab., 57 (1997) 135.
17 L. H. Perng, C. J. Tsai and Y. C. Ling, Polymers, 40 (1999) 7321.
18 J. P. Lin, C. Y. Chang and C. H. Wu, J. Hazard. Mat., 58 (1998) 227.
19 K. S. Lin, H. P. Wang, S. H. Liu, N. B. Chang, Y. J. Huang and H. C. Wang, Fuel Proc. Tech., 60 (1999) 103.